Geomorphology 506 (2026) 110332

Contents lists available at ScienceDirect

Geomorphology

journal homepage: www.journals.elsevier.com/geomorphology

Corrigendum

Corrigendum to "Advantages of integrated geophysical, sedimentary, and dating approaches for reconstructing Holocene tidal inlet evolution: A case study from offshore the Belgian coastal plain" [Geomorphology 505 (2026) 110311]

Víctor Cartelle [a,*], Soetkin Vervust [b], Wout Van Wesemael [c,d], Thomas Mestdagh [a], Yağız Arda Çiçek [e], Christian Schwarz [e,f], Tine Missiaen [a], Marc De Bie [b], Ruth Plets [a]

[a] Flanders Marine Institute (VLIZ), Jacobsenstraat 1, 8400, Oostende, Belgium
[b] Vrije Universiteit Brussel, Archaeology, Environmental Changes, and Geo-Chemistry (AMGC), Pleinlaan 2, 1050, Brussels, Belgium
[c] KU Leuven, Faculty of Medicine, Department of Oral Health Sciences, Kapucijnenvoer 7, 3000, Leuven, Belgium
[d] KU Leuven, Faculty of Engineering Science, Department of Materials Engineering, Kasteelpark Arenberg 44, 3001, Leuven, Belgium
[e] KU Leuven, Department of Civil Engineering, Kasteelpark Arenberg 40, 3001, Leuven, Belgium
[f] KU Leuven, Department of Earth and Environmental Sciences, Celestijnenlaan 200E, 3001, Leuven, Belgium

The authors regret that the printed version of the above article contained a number of errors. The correct and final version follows. The authors would like to apologise for any inconvenience caused.

Abstract

Relict tidal inlets preserved on continental shelves provide key evidence for past shoreline positions and coastal evolution, but their recognition is often hindered by erosion, reworking and fragmentary preservation. Here we integrate high-resolution sub-bottom profiling, sedimentological facies analysis, radiocarbon dating, and optically stimulated luminescence (OSL) profiling to reconstruct the mid- to late Holocene evolution of a tidal inlet complex located offshore the Belgian coastal plain. Six major channels (A–F) were acoustically mapped and linked to sediment cores, revealing channel fills, lateral-accretion packages, and prograding sand body deposits. Luminescence profiling of cores established a relative chronostratigraphy that, once anchored to radiocarbon dates and stratigraphic relationships, resolved anomalous ages and refined the chronology of channel activity. Results indicate that all of these mapped channels correspond to repeated phases of tidal inlet incision, migration, and reoccupation within a confined coastal sector over a period of at least four millennia. The preserved stratigraphy demonstrates that the inlet complex remained fixed in broadly the same position relative to the current shoreline between 5.6 ka and 1.7 ka BP. This implies that the coastline and its associated barrier system persisted at approximately 2 km seaward of the present-day coastline for about 4000 years, despite sea-level rise and transgressive erosion. These findings provide the first offshore evidence complementing and challenging reconstructions from land-based studies of the Belgian coastal plain. This approach also allows to reconstruct former coastline and tidal inlet positions in partly reworked offshore settings. More broadly, they demonstrate how integrating geophysical imaging, sedimentary facies, radiocarbon dating and OSL profiling can overcome the limitations of classic approaches by resolving reworked ages, constraining inlet mobility, and delivering more robust palaeogeographic reconstructions of Holocene coastal change.

Keywords

Palaeo-tidal inlets
Optically stimulated luminescence profiling
Acoustic data
Palaeocoastline reconstruction

1. Introduction

Tidal inlets are openings along barrier coasts through which tidal currents enter and exit, connecting lagoons, marshes and tidal creek systems to the open sea (FitzGerald et al., 2012). These are highly dynamic systems, characterised by the confluence of tides, waves and storms creating cross- and long-shore sediment transport patterns over different spatio-temporal scales which govern water and sediment

DOI of original article: https://doi.org/10.1016/j.geomorph.2026.110311.
* Corresponding author.
E-mail address: victor.cartelle@vliz.be (V. Cartelle).

https://doi.org/10.1016/j.geomorph.2026.110332

Available online 20 April 2026

exchange through the barrier. Inlet-barrier systems are typically present on mixed-energy coastlines where the relative influence of waves and tides governs the general morphology; when tides dominate these mixed energy systems, well-developed tidal inlets and extensive associated ebb- and flood tidal deltas are present (Davis and Hayes, 1984). Inlet morphologies evolve in response to variations in sediment supply, hydrodynamic conditions, upstream freshwater input and sea-level change (De Haas et al., 2018; FitzGerald et al., 2012; FitzGerald and Miner, 2013). They usually represent the deepest part of barrier-inlet systems and, consequently, have a high preservation potential, although their associated deposits are usually only fragmentary (Belknap and Kraft, 1981, 1985; Rieu et al., 2005). Still, the relict tidal inlets often represent the only sedimentary evidence for recognising ancient barrier-inlet systems and reconstructing past shoreline positions, as the shallower elements are often removed by later erosion (Belknap and Kraft, 1981, 1985; FitzGerald et al., 2012). Therefore, reliable reconstructions of relict tidal inlets are essential: they help us understand the long-term development of past coastal systems, identify the parameters that control their geological evolution and improve our ability to recognise ancient barrier-inlet systems in the geological record. They also provide valuable insights for anticipating how comparable systems may respond to future environmental change. In areas with a long history of human intervention, they may further help in revealing the relative roles of natural versus anthropogenic forcing on the development of tidal systems, supporting more informed management and forecasting efforts (Baeteman, 2018; De Haas et al., 2018).

Relict tidal inlet systems have been documented in several continental shelves worldwide (e.g., Hein et al., 2012; Hollis et al., 2019; Rieu et al., 2005; Ronchi et al., 2018, 2019; Storms et al., 2008). However, their recognition in the sedimentary record remains limited, and most understanding of inlet morphodynamics and facies architecture is derived from modern analogues governed by a limited combination of forcings which may not be universally applicable. The identification and characterisation of evidence of the former coastline positions on continental shelves is also challenging because they have been subject to significant erosion due to transgressive ravinement processes (Allen and Posamentier, 1993; Cattaneo and Steel, 2003; Demarest and Kraft, 1987; Nummedal and Swift, 1987; Swift, 1968; Zecchin et al., 2019; Zecchin and Catuneanu, 2013), or have been altered by human activities over the last centuries. Consequently, the stratigraphic record is frequently fragmentary and incomplete. In addition, preserved environmental signals in such a dynamic setting may have undergone multiple cycles of reworking, with large-scale changes happening at decadal and centennial scales (Bienzobas Montávez et al., 2024; Cartelle et al., 2022; De Francesco and Hassan, 2008; Muñoz Sobrino et al., 2024; Romans et al., 2016; Toby et al., 2022). Most reconstructions rely on individual datasets such as seismic geomorphology, sediment facies analysis, or radiometric dating, each of which provides only a partial view. These complexities and challenges introduce uncertainties in palaeogeographic reconstructions that can only be addressed through integrated approaches. Specifically, high-resolution geophysical imaging constrains the geometry and spatial continuity of sediment bodies, sedimentological analysis resolves depositional environments, and independent chronological datasets establish temporal relationships between units. Combining these datasets allows cross-validation between methods, helps distinguish primary depositional signals from reworked material, and permits the reconstruction of shoreline evolution even where erosion, data gaps, or stratigraphic incompleteness would render individual datasets inconclusive.

In this study, we reconstruct the evolution of a relict tidal inlet system to better understand the long-term development of the Belgian coastal plain during the Holocene. By integrating high-resolution geophysical imaging, sedimentary facies analysis, and multiple independent dating methods, we resolve the spatial organisation and temporal evolution of inlet activity preserved in the nearshore zone. The Belgian coastal plain provides an exceptional case study, with well-preserved Holocene deposits offering a rare opportunity to investigate the dynamics of a relict barrier-inlet system and its response to changing environmental conditions. Novel in our approach for a coastal setting is the application of optically stimulated luminescence (OSL) profiling to unravel the complex stratigraphic architecture and to build a three-dimensional relative chronostratigraphic framework, anchored to an absolute chronology using radiocarbon dating. This approach allows us to identify stratigraphic relationships and chronological inconsistencies that would otherwise remain unresolved, thereby strengthening the reconstruction of inlet evolution and associated coastal change.

2. Study area

The Belgian coastal plain represents a unique landscape shaped by the interaction of natural processes and human activities. It was once a dynamic tidal environment of channels, mudflats, dunes and salt marshes, but has now been transformed into a densely populated and developed region with a shoreline with coastal defences. The interaction between past environmental conditions, the palaeogeomorphology and the strategies developed by people to live in this coastal landscape, has been pivotal in shaping the present-day coastal system (Baeteman, 1999; Baeteman et al., 2002; Baeteman, 2005, 2018; Baeteman and Declercq, 2002; Denys and Baeteman, 1995; Tys, 2013). Research into the coastal evolution has mainly focused on the onshore side. Whilst detailed studies on land, including sedimentology, dating and palaeoenvironmental proxies, have led to a good understanding of the Late Pleistocene and Holocene coastal evolution, offshore reconstructions are mostly based on hypotheses and secondary evidence from regional seismic data (De Clercq, 2018; Mathys, 2009).

Offshore, the Quaternary record of the continental shelf has mainly been studied using a seismostratigraphic approach based on regional seismic profiles of mid to low resolution (typically ~1 m vertical resolution). It comprises a relatively thin and complex patchy sediment cover of Late Pleistocene and Holocene age (De Clercq, 2018; Mathys, 2009) overlying thick Palaeogene deposits, mainly composed of compacted, folded and faulted clays and sands to sandy clays, deposited in a near-coastal to shelf environment (De Batist, 1989; Henriet and De Moor, 1989; Le Bot et al., 2003). Mathys (2009) proposed that the Holocene flooding of the Belgian continental shelf led to the formation of linear coastal barriers that migrated landward and seaward in response to changes in sea level and accommodation space, but most of these deposits were eroded and reworked by the marine transgression.

Research on land on the other hand, has revealed that the western Belgian coastal plain was flooded by 9400 cal a BP through the IJzer palaeovalley (Fig. 1), which led to the formation of an estuary with tidal channels and flats fringed by freshwater environments where peat accumulated (Baeteman, 1999). As sea level rose, the coastal plain evolved into a barrier system by 8000–7800 cal a BP (Baeteman and Declercq, 2002). Rapid sea-level rise (SLR) during the Early Holocene (ca. 7 m/kyr, Denys and Baeteman, 1995) is believed to have led to a rapid retreat of the coastal barrier until 7500–7000 cal a BP, after which the rate of SLR decreased (ca. 2.5 m/kyr, Denys and Baeteman, 1995). This reduced SLR rate promoted higher coastal stability by 6800 cal a BP, while the tidal basin reached its maximum landward extent around 6300 cal a BP (Baeteman and Declercq, 2002). A further deceleration in sea-level rise around 5500–5000 cal a BP (ca. 0.7 m/kyr, Denys and Baeteman, 1995) led to a phase of shoreline progradation and contraction of the tidal channel network. At this point, the coastal plain evolved into a freshwater marsh with associated peat formation (Baeteman, 1999; Baeteman and Declercq, 2002). The Late Holocene was characterised by the return of the tidal system to the coastal plain with the renewed incision of mid-Holocene tidal channels after 2800 cal a BP, though the drivers behind this change remain unclear (Baeteman, 2005; Baeteman et al., 2002). By 1400–1200 cal a BP, most of the coastal plain had silted up, evolving into supratidal environments. Only the larger tidal channels remained open, until broadscale embankment started by

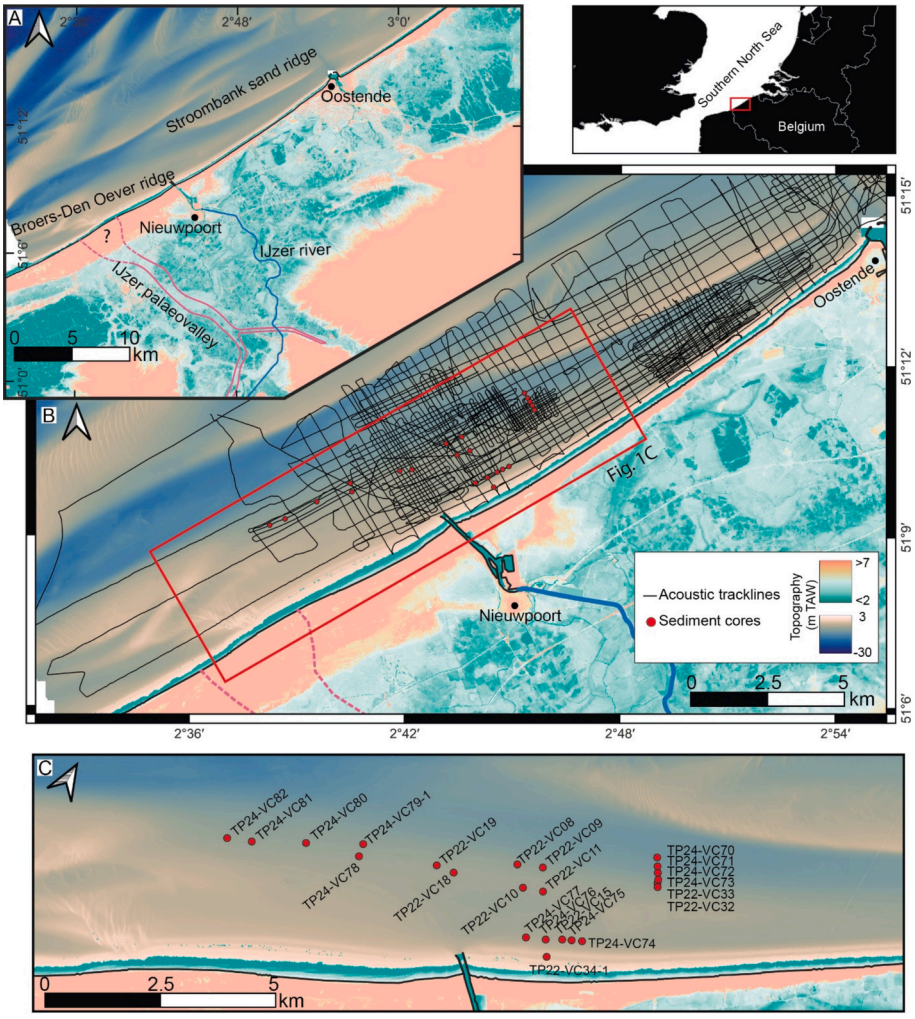

Fig. 1. *A) Location of the study area at the Belgian Middle coast, showing the main cities, the river IJzer and the Early Holocene IJzer palaeovalley (*Baeteman and Declercq, 2002*). B) Overview of all data collected in the study area, including high-resolution acoustic profiles and vibrocores. C) Detailed location of the sediment cores for the area within the red rectangle shown on B. Background bathymetric data was provided by Agentschap Maritieme Dienstverlening en Kust and is available at* www.agentschapmdk.be*. Topographic data was developed by Nationaal Geografisch Instituut and is available at* www.geo.be.

1000 cal a BP, which eventually led to the present-day polder landscape (Tys, 2013).

In this study, we investigate the nearshore zone of the western and central Belgian coastal plain, roughly between the French-Belgian border to the west and the current location of the city of Oostende to the east (Fig. 1). The investigated area covers about 200 km^2, spanning 33 km of coastline and up to 6.6 km offshore. Today, this sector is characterised by a narrow sandy beach bordered by either a promenade with high-rise buildings or a strip of dunes. The shallow subtidal zone displays a swale and ridge morphology of large shoreface-connected sand ridges, with the Broers-Den Oever ridge to the west and the Stroombank ridge to the east (Fig. 1). The main river draining this part of the coast is the river IJzer (Fig. 1). Its mouth in Nieuwpoort is now canalised and managed by sluice gates, draining a small and low-lying basin in the coastal plain. The region experiences a macro-tidal regime, with tidal range decreasing from southwest to northeast; the mean tidal range at Nieuwpoort is 4 m (Verwaest et al., 2022).

3. Methods

Acoustic and sedimentary datasets were acquired during ten offshore surveys between January 2022 and June 2024 using the R/V *Simon Stevin* and the dive vessel *Last Freedom*. Each type of data will be discussed below in greater detail.

3.1. Acoustic data

Acoustic data were acquired using a parametric sub-bottom profiler model SES-2000 Quattro (Innomar Technologie GmbH), operating in single-beam mode at a frequency of 8 kHz (2023 and 2024) or 10 kHz (2022). Positioning information was recorded through input from an RTK GNSS system, whereas an auxiliary motion reference unit allowed online heave corrections. After conversion from Innomar's proprietary data format (.ses3) to seg-y, vertical variations due to the tidal range were corrected using RadExPro, and all profiles were referenced to the Belgian datum (Tweede Algemene Waterpassing, TAW) corresponding to the mean lower low tide in Oostende, which is ca. 2.33 m below the present mean sea level. The interpretation of acoustic facies and units followed standard principles of seismic stratigraphy (Mitchum Jr., 1977; Mitchum Jr. et al., 1977; Mitchum Jr. and Vail, 1977). Key horizons were mapped and gridded using the flex gridding algorithm of the S&P Global-Kingdom v. 2023 software. The infill between key horizons was characterised by their acoustic facies and tied to relevant sediment cores at targeted locations. For time to depth conversion an average sound velocity of 1600 m/s for the sediment was used. Core compaction was corrected when possible, by calculating the ratio between total core penetration and core recovery. Facies transitions within the cores were assumed to correspond to the highest acoustic impedance contrasts, resulting in traceable reflections on the acoustic profiles.

3.2. Sediment cores

The vibrocorer (Ocean Scientific International Ltd) consisted of a 3-m long, 9-cm-diameter steel core barrel equipped with a high-power vibrating motor (>100 kN). The coordinates of the location of the cores are included in Supplementary Material (Table S1). In the lab, the sediment cores were split lengthwise under red-light conditions to keep them light-safe, then photographed and described. Grain size was logged visually by comparison with a grain-size scale and selected samples were analysed for detailed grain-size distributions by laser diffraction using a Malvern Mastersizer 3000 at Ghent University after treatment with H_2O_2 and HCl to remove organic and calcium carbonate content. Grain size classes followed Wentworth (1922). For the lithofacies definition (Supplementary Material, Table S2), we adopted the standardised classification of Farrell et al. (2012), recognising heterolithic interbeds where high-frequency couplets of mm- to cm-scale laminae and beds were present.

3.3. Absolute and relative dating

Radiocarbon dating was used to establish the chronological context of the seismic units. Both well-preserved shell valves and peat samples were analysed at the Beta Analytic Laboratory (USA) and the radiocarbon laboratory of the Royal Institute for Cultural Heritage (KIK-IRPA, Belgium). All radiocarbon dates were calibrated using Calib Rev. 8.2 (Stuiver and Reimer, 1993) and are reported as cal a BP (2σ confidence level). The Marine20 calibration curve (Heaton et al., 2020) and the IntCal20 calibration curve (Reimer et al., 2020) were used for the bivalve shells and peat samples, respectively.

Because estuarine–tidal systems show complex, rapidly changing facies and frequent reworking, single-point ages through radiocarbon or OSL dating can be misleading if the dated material is residual (radiocarbon) or incompletely bleached (OSL), leading to age overestimation. Absolute dating is also labour- and cost-intensive. To address these challenges, bulk OSL profiling was applied as a complementary, relative dating technique. It acts as an efficient screening tool, offering a rapid, low-cost approach to assess and compare the luminescence characteristics of large numbers of samples. These can then be used to anchor absolute dates into larger relative chronological frameworks. OSL profiling was performed on selected sand deposits following the methodologies described by Munyikwa et al. (2021) and Sanderson and Murphy (2010). We used the portable luminescence reader developed by the Scottish Universities Environmental Research Centre (SUERC), equipped with infrared (880 ± 40 nm) and blue (470 ± 20 nm) LEDs for signal stimulation, UG11 filters and a 25 mm bi-alkali photomultiplier for signal detection (Sanderson and Murphy, 2010). Poly-mineral bulk sediments (ca. 50 g) collected from target sands were measured without pretreatment using the preset continuous-wave (CW) proxies stimulation sequence: 15 s dark count, 2 × 30 s infrared stimulation (IRSL), 15 s dark, 2 × 30 s blue light stimulation (OSL), 15 s dark. The luminescence signal is measured in photon counts per second.

Several proxies can be calculated from these measurements (Munyikwa et al., 2021; Sanderson and Murphy, 2010). The primary ones are the net IRSL and OSL signal intensities, computed as the total photon count over the IRSL and OSL measurement cycle minus the preceding and following dark count. Net IRSL and OSL signals can be influenced by dose rate, inherited luminescence at burial, luminescence sensitivity, mineralogy and time since burial. When most of these variables are similar across samples, the signal intensity acts as a proxy for age. We also calculated depletion indices for IRSL and OSL—the proportion of signal released in the first half of the stimulation cycle relative to the second half—as indicators of sample transparency and bleaching state, helping to identify inherited versus single irradiation cycle signals. Finally, the IRSL/OSL ratio provides a proxy for mineralogical variation (feldspar- versus quartz-dominated contributions). To reduce sources of variability in luminescence signals, we only targeted sand deposits within the channel complex and avoided disturbed or bioturbated sediments, and layers rich in clay and silt. Under these constraints, we interpret higher IRSL and OSL signal intensities as indicating older deposits. No OSL dating was carried out for the cores used in this study, but OSL profiling and dating we performed on other cores from the study area had shown this to be a valid assumption (Vervust et al., 2025). The full OSL profiling measurements are provided in Supplementary Material (Table S3).

4. Results and interpretation

4.1. Recognition of channel facies

The analysis of the acoustic data from the nearshore area offshore Nieuwpoort allowed the identification of laterally extensive acoustic facies that define the overall stratigraphic architecture of the nearshore sedimentary succession (Fig. 2). Mapping of the different facies reveals extensive deposits associated with channel-like incisions along 10 km of coastline. We distinguish two types of channel elements*: channel fills* and *lateral-accretion packages*. These architectural elements are bounded by concave-up erosive surfaces at their base, and subhorizontal disconformities at their top (Fig. 3).

In the acoustic profiles, *channel fills* appear as concave-up deposits forming elongated troughs with irregular geometries (Figs. 3 and 4). Their bases are marked by erosional surfaces that truncate underlying units, while their internal architecture consists predominantly of subhorizontal to gently inclined, parallel reflections that onlap onto the channel margins, a geometry consistent with aggradational infill. Two end-member geometries can be recognised: symmetric fills (acoustic facies f1, Fig. 2), where reflections are evenly developed on both channel flanks to form subhorizontal packages; and asymmetric fills (f2, Fig. 2), where reflections remain continuous across the channel but show contrasting geometries, being horizontal to subhorizontal on one flank and dipping towards the thalweg on the opposite flank. A total of six channel fills have been mapped in the study area, labelled A to F from northeast to southwest (Fig. 4).

Adjacent to some channels, clinoform reflections form distinct lateral-accretion packages (Fig. 3). These occur in sets with predominantly oblique-tangential configurations (f3, Fig. 2), where individual reflections converge downwards into the thalweg. Their geometry reflects the direction of lateral channel migration, while their systematic stacking suggests sustained channel activity (Figs. 3, 5 and 6).

In addition to the channelised facies, laterally extensive units occur both between and locally overlying the channel fills. These deposits also display prograding clinoforms but are bounded at the base by flat, subhorizontal surfaces. We interpret them as *prograding sand body deposits*, representing a distinct facies group from the channel fills (Fig. 3). They are typically characterised by subparallel reflections that downlap onto the underlying surfaces (dip 0.6–3.5°), with a predominantly oblique-parallel configuration (f4, Fig. 2). Clinoform sets indicate progradation parallel to the present-day coast or in a landward direction to the southeast. Some of these prograding sand body deposits are cut by the channels (e.g., channels F and A in Figs. 3 and 5), which can complicate their distinction from lateral-accretion packages. However, their local occurrence above channel fills (e.g., channels E and B in Figs. 3 and 7) confirms their status as discrete architectural elements.

4.2. Sedimentary facies

A total of 34 sedimentary facies were identified in the cores, both as part of the channel fills, the lateral accretion packages and the prograding sand body deposits. These include gravel-, sand- and mud-dominated facies, heterolithic lamination and bedding, as well as peat. Detailed facies descriptions are provided in Supplementary Table S2, and their distribution along the cores is shown in Figs. 3, 5, 6 and 7. Additional core logs are included in Supplementary Material (Fig. S1).

Acoustic facies	Amplitude	Frequency	Continuity	Refl. termination	Configuration	Example	Interpretation
f1	Medium High	Medium High	High	Top: truncation Base: onlap	Parallel, horizontal, channelised symmetric	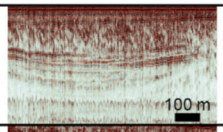	Channel fill
f2	Medium High	Medium High	High	Top: truncation Base: onlap	Parallel, channelised asymmetric	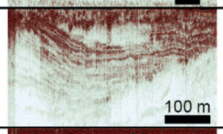	Channel fill
f3	Medium	Low	Medium	Top: truncation Base: downlap	Oblique-tangential	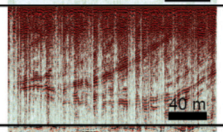	Channel migration
f4	Medium	Low	Medium	Top: truncation Base: downlap	Oblique-parallel	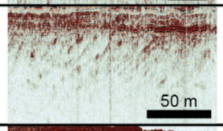	Deposits of tidal deltas
f5	Low	Low	Low	NA	Semi-transparent	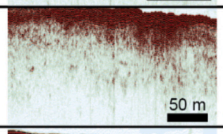	Gas in the sediment
f6	High	Medium	High	NA	Parallel	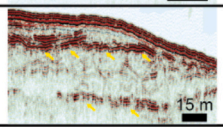	Peat deposits

Fig. 2. Acoustic facies identified in the study area.

4.3. *Morphology and infilling geometry of channels*

In the study area, we identified six offshore channel fills (A-F, labelled from East to West) with associated lateral-accretion packages (Fig. 4). These features can be traced from the present-day coastline to approximately 3.0–3.5 km offshore, along at least 10 km of coast. In some areas the presence of gas in the sediment (f5, Fig. 2) causes acoustic blanking, making it difficult to map the full extent of the channel fills (Fig. 4). The main morphological characteristics of the channels are summarised in Table 1.

Channel A is the easternmost channel fill. Its mapped width covers at least 2.8 km, running almost parallel to the present-day coast at a distance of 2 km (Fig. 4). Multiple phases of cut and fill can be distinguished, with both symmetric and asymmetric channel fills (Fig. 5). The deepest incision reaches 18.6 ms TWT (ca. −14.9 m TAW, Figs. 4 and 5). Lateral-accretion packages indicate some southward channel migration towards the coast. Channel A cuts and runs parallel to an extensive prograding sand body composed of multiple clinoform sets, also indicating landward progradation (Fig. 5). A transect of sediment cores (Figs. 5) shows a dominance of laminated sand facies (S_{lam}, $S_{lam\text{-}biot}$) with some thick gravel deposits (mxd sG-m) associated with the prograding sand body, and laminated sands (S_{lam}) with mud interbeds (S/M_f) associated with the lateral accretion. Channel deposits are dominated by heterolithic facies (e.g., S/M_{lam}, S/M_w). Radiocarbon ages from core TP22-VC33 indicate an age of 6055–6375 cal a BP for the channel fill (Table 2, Fig. 5).

Channel B is the deepest channel in the area, extending up to 3.3 km offshore. It is coast-perpendicular nearshore, and curves into an almost coast-parallel orientation further offshore (Fig. 4). It reaches a maximum depth of 23.2 ms TWT (ca. -18.6 m) in the nearshore coast-perpendicular sector, and 27.0 ms TWT (ca. -21.6 m) in the coast-parallel sector (Fig. 4), where it also cuts into older deposits (Fig. 7). Its longitudinal topographic profile is irregular, with three points of maximum depth (Fig. 4). Channel fills vary between symmetric (Fig. 7) and asymmetric (Fig. 6), while thick and extensive lateral-accretion packages indicate eastward and northeastward migration (Figs. 4 and 6). Offshore, this channel is covered by thick landwards prograding sand body deposits which are laterally extensive and cut by shallower channels (Fig. 7). Sedimentary facies were only recovered for the last phase of cut and fill preserved in its proximal area and show that the channel is fringed by peat and muddy facies (e.g. TP24-VC75, Fig. 6). Radiocarbon dating of the peat deposits in TP24-VC75 provided an age of 7705–7930 cal a BP (Table 2, Fig. 6). These peat layers are laterally extensive along the coast and appear in acoustic profiles as continuous, high-amplitude reflections (f6, Figs. 2 and 6). The lateral-accretion package associated with channel B records a fining-upwards sequence (TP24-VC77, Fig. 6), from basal bioclastic and siliciclastic gravels (mxd sG-m) to laminated fine to medium sands (S_{lam}, $S_{lam\text{-}org}$) and heterolithic bedding (S/M/P_{lam}). Eastward, it passes into laminated or structureless sands with mud interbeds (e.g., S_{lam}/$M_{m\text{-}org}$, mxd gS_{lam}, S_m) within the main oblique-tangential clinoform sets (Fig. 6). The youngest preserved fills of channel B are characterised by sub-horizontal asymmetric parallel reflections composed of shell-rich laminated sands (S_{lam}), and mud and sand interbeds (M/S_{lam}). One radiocarbon date indicates an age for these deposits of 5445–5750 cal a BP (Table 2, Fig. 6).

Channel C occupies the shallowest stratigraphic position, forming a north-south depression, 2 km long and 1 km wide, overlying or cutting channels B and D (Fig. 4). Its base reaches 18.5 ms TWT (ca. -14.8 m). Lateral-accretion packages denote a change in the direction of lateral accretion over time, from east-to-west direction (Figs. 4 and 6) to west-to-east direction (Fig. 4). Sedimentary facies are dominated by laminated muddy fine and medium sands (mS_{lam}, Fig. 7). Radiocarbon dating indicates an age of 1565–1875 cal a BP for the youngest preserved infill of this channel (Table 2, Fig. 7).

Channel D displays a similar filling pattern as channel C, cutting down to 18.1 ms TWT (ca. -14.5 m). It has a symmetric channel fill and a thick lateral-accretion package indicating east-to-west migration (Fig. 4). Sedimentary facies are again dominated by laminated muddy

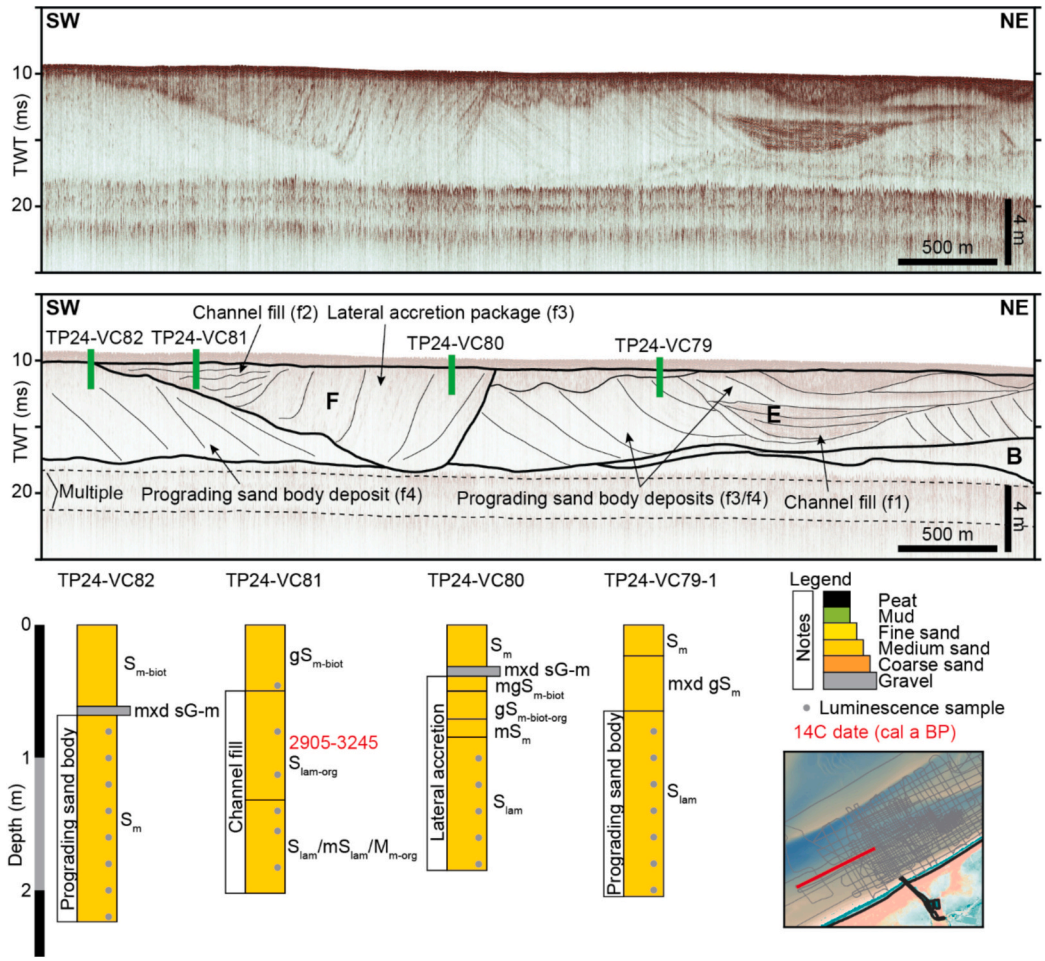

Fig. 3. High-resolution acoustic profile across the study area showing the channel-like incisions identified in the study area (channels E and F) characterised by channels fills and lateral-accretion packages, and associated with extensive prograding sand body deposits. Representative sediment cores are also shown. For the codes of the sedimentary facies refer to Supplementary Table S2. Luminescence samples were used for OSL profiling.

sands (mS_{lam}, Fig. S1).

Channels E and F in the westernmost part of the study area are associated with extensive prograding sand body deposits (Fig. 3). Channel E is a 3-km-long, shore-parallel depression reaching 16.6 ms TWT (ca. -13.3 m, Figs. 3 and 4). Sediment cores did not reach the channel fill, but acoustic data show a symmetric, high-amplitude reflector pattern (Fig. 3). Channel F further to the west is one of the most extensive features in the area (2.2 km long, 2 km wide), but its mapping is limited by the lower spatial resolution of acoustic profiles and the presence of extensive areas of acoustic blanking in the sediment (Fig. 4). It reaches a maximum depth of 19.7 ms TWT (ca. -15.8 m) and is associated with a thick lateral-accretion package that indicates east-to-west channel migration and shallowing (Fig. 3). Sedimentary facies mainly correspond to laminated and structureless muddy and gravely sands ($mgS_{m\text{-}bio}$, $gS_{m\text{-}bio\text{-}org}$, mS_m, S_m, S_{lam}). A radiocarbon date obtained from core TP24-VC81 indicates an age of 2905–3245 cal a BP for the channel fill (Table 2, Fig. 3).

4.4. Luminescence profiling of channel deposits

The luminescence measurements from the main channel deposits show a wide range of net OSL signal intensities, from 178×10^3 counts in TP22-VC08 to more than 1.9×10^6 counts in TP24-VC76 (plotted in reverse scale to reflect stratigraphic position in Fig. 8A). The highest values ($>12 \times 10^6$ counts) occur in deposits underlying channels A and B, recovered at the base of cores TP22-VC33 and TP24-VC75 (Figs. 5, 6 and 8A). A clear geographical pattern emerges when the cores are arranged from southwest to northeast, denoting several clusters with similar signal intensities (Fig. 8A). Each cluster corresponds to one or two channel fills. The highest values are associated with sediments from the top of channel fill B, the deepest and largest channel, ranging from 880×10^3 to 1.9×10^6 counts (cores TP22-VC15 and TP24-VC76, Figs. 6 and 8A). Comparable intensities are observed in the area of channel A, ranging between 521×10^3 and 1.4×10^6 counts (cores TP24-VC70 and TP22-VC32, Figs. 5 and 8A).

In the sector of channel fills E and F, signal intensities are generally lower, between 380×10^3 and 1×10^6 counts. Within this group, cores TP24-VC78 and TP24-VC79 of channel E yield slightly higher values than TP24-VC80 and TP24-VC81, where the upper fill of channel F has lower values (Figs. 3 and 8A). The lowest values are associated with the infill of channel C, typically below 426×10^3 counts (Fig. 8A). Sediments from channel D show intermediate values, higher than those of channel C but broadly comparable to channel F (Fig. 8A).

The IRSL/OSL ratios and the IRSL and OSL depletion indices show little geographical variation (Fig. 8B, C). The IRSL/OSL ratio remains consistent across the entire study area, with an average value of 0.14 ± 0.02, suggesting little variation in sample mineralogy (Sanderson and Murphy, 2010). The IRSL and OSL depletion indices are relatively high and similar across most cores, with average values of 1.27 ± 0.05 and 1.86 ± 0.11, respectively. These values indicate broadly similar bleaching characteristics across the area (Sanderson and Murphy, 2010).

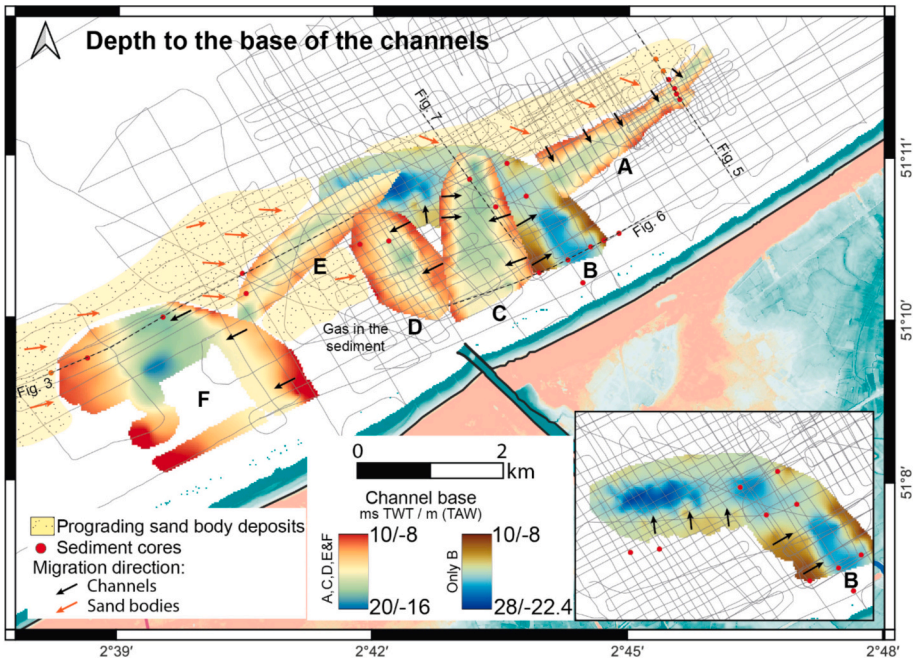

Fig. 4. Map of channels and prograding sand body deposits identified in the study area. Depth (in ms TWT and m TAW) corresponds to the disconformity identified at the base of channel fills and lateral-accretion packages. Arrows indicate the migration direction deduced from lateral-accretion packages and prograding sand body deposits. Note that a different colour scale is used for channel B. The location of the profiles included in Figs. 3, 5, 6 and 7 are also shown.

4.5. Interpretation of the channels

The channels identified offshore Nieuwpoort display morphological and sedimentological characteristics of tidal inlet systems. Their elongated trough-like geometry, with concave-up thalweg profiles that shallow both landward and seaward, contrasts with typical fluvial channels and instead indicates localised scouring and flow constriction (Paquet et al., 2023). Internally, the fills consist of laterally accreting packages and multi-storey channel deposits with abundant heterolithic facies, marine shells, and faunal remains, all pointing to tidal processes rather than persistent fluvial input.

The abrupt seaward termination of the channels, where their bases become progressively shallower, is consistent with the geometry of ebb-tidal channels incising coastal barriers (FitzGerald et al., 2012; FitzGerald and Miner, 2013). Similar morphologies and facies have been documented in preserved inlet fills offshore the western Netherlands (Rieu et al., 2005), the northern Adriatic (Ronchi et al., 2019; Storms et al., 2008), and other continental shelves worldwide (Hein et al., 2012; Hollis et al., 2019). In such settings, only the deepest parts of the inlet channels are commonly preserved because ravinement and barrier overstepping removed shallower elements, which explains the patchy and fragmentary character of the deposits. The association of heterolithic tidal facies, shell-rich lags, and large-scale lateral accretion observed here closely matches the facies models of modern and ancient tidal inlets (e.g., FitzGerald et al., 2012), lending further support to our interpretation of these channels as relict tidal inlets. Taken together, the evidence suggests that the channels located offshore Nieuwpoort represent the remains of large Holocene tidal inlets that connected the back-barrier basin of the Belgian coastal plain to the North Sea.

In addition to the channel fills and lateral-accretion packages, we identify prograding sand body deposits preserved both seaward of and laterally adjacent to the channels. These are interpreted as inlet-associated sand bodies, including sandy platforms developed seaward of the inlet throat under ebb-dominated tidal currents and subsequent reworking by waves, as well as deposits formed along the lateral margins of the inlet through barrier or spit accretion. Their fragmentary preservation is consistent with later ravinement and offshore redistribution, processes that typically erode such sand bodies in coastal settings (Belknap and Kraft, 1981, 1985).

4.6. Age of the channels

To establish the chronology of the channels, we interpreted the luminescence signals in conjunction with stratigraphic relationships and available radiocarbon ages (Fig. 8A). As outlined in Section 4.4, most samples display comparable mineralogical and bleaching characteristics, as indicated by the IRSL/OSL ratio and the IRSL and OSL depletion indices (Fig. 8B, C). This consistency allows net OSL signal intensities to be used as a relative age proxy, with higher counts interpreted as older and lower counts as younger deposits. This relative framework was anchored to an absolute timescale using selected radiocarbon dates (Table 2) and quality-checked against stratigraphic relationships. Together, this helped resolve reworked radiocarbon ages and refined the sequence of channel activity. In the following paragraphs, we use this integrated approach to reconstruct the relative timing of incision and infill for channels A to F.

Luminescence profiling shows that vertical successions of net OSL counts within individual cores are relatively consistent, whereas much larger variations occur between different cores (Fig. 8A). Channel B has the highest luminescence values of all the channels, although only the upper deposits were sampled, representing the youngest preserved infill. Cores TP24-VC76 and TP22-VC15 recorded the highest values within B, corresponding to the lateral accretion package and the channel fill respectively (Figs. 6 and 8A). This is followed by values recorded in TP22-VC09, which was recovered from the prograding sand body deposits offshore covering the channel B fill (Fig. 7). Comparable luminescence values were obtained from channel A to the east of B (cores TP22-VC32 and TP22-VC33, Fig. 8A). The parallel orientation of channel A to the coast and its stratigraphic position suggest that it functioned as a marginal branch contemporaneous with the main channel B. Radiocarbon dates support this interpretation, with ages of 5445–5750 cal a BP (channel B) and 6055–6375 cal a BP (channel A). An older peat age of 7705–7930 cal a BP from TP24-VC75 likely constrains eastward migration of channel B closer to the present-day coast, as these peat

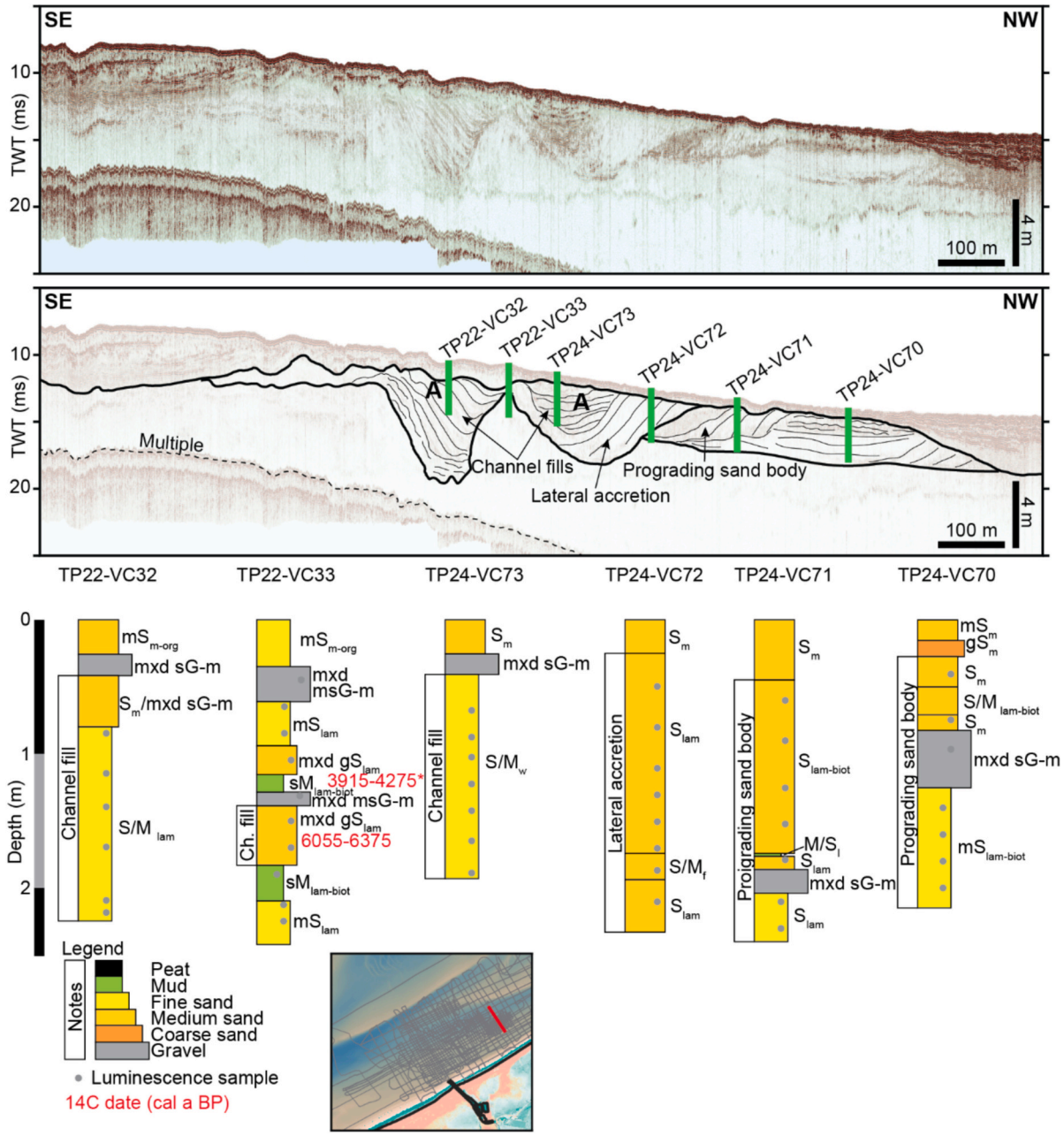

Fig. 5. High-resolution acoustic profile across the study area showing channel A and representative sediment cores. For the codes of the sedimentary facies refer to Supplementary Table S2. Luminescence samples were used for OSL profiling. The * indicates a radiocarbon date interpreted as reworked. Pictures of representative cores are included in Supplementary Material (Fig. S2).

deposits are cut by the channel (Fig. 6). Deposits underlying these channels, recovered in cores TP22-VC33 and TP24-VC75, yielded the highest luminescence values in the study area (>12 × 10^6 counts, Fig. 8A). There are no absolute ages for these deposits, but given that their net OSL values are an order of magnitude greater than the highest values recorded for the channels, we interpret them as the offshore continuation of the extensive Pleistocene deposits along the Belgian coastal plain (Bogemans et al., 2016). Overall, these results indicate that channel B represents the oldest and deepest preserved tidal inlet within the complex, while channel A marks a smaller and shallower offshore coast-parallel marginal branch.

The relative chronology then points to a westward shift of the inlet system. High values in channel E, closely followed by channel F, indicate these inlets formed after channel B (Fig. 8A). Sub-bottom and core evidence suggest that both channels are closely related, with channel E likely continuing coastward along a pathway later reoccupied by channel F (Fig. 4). TP24-VC82, with values consistent with channel E, supports this interpretation (Fig. 8A). Within this sequence, channel F has the lowest luminescence intensities, identifying it as the youngest preserved inlet to the west. This conclusion is corroborated by the radiocarbon age of 2905–3245 cal a BP from its upper fill (Fig. 3).

Finally, luminescence values decrease from west to east across channels D and C, indicating a later reoccupation of the eastern sector. Here, several radiocarbon ages appear inconsistent with the luminescence chronology. For instance, the ages 6600–6935 cal a BP from channel D (core TP22-VC18) and 5745–6095 cal a BP from channel C (core TP22-VC09) are older than any radiocarbon ages from channels with higher luminescence values and are therefore interpreted as reworked (Fig. 8A, Table 2). Similarly, radiocarbon dates from the upper sediments of cores TP22-VC33 (3915–4275 cal a BP) and TP22-VC34

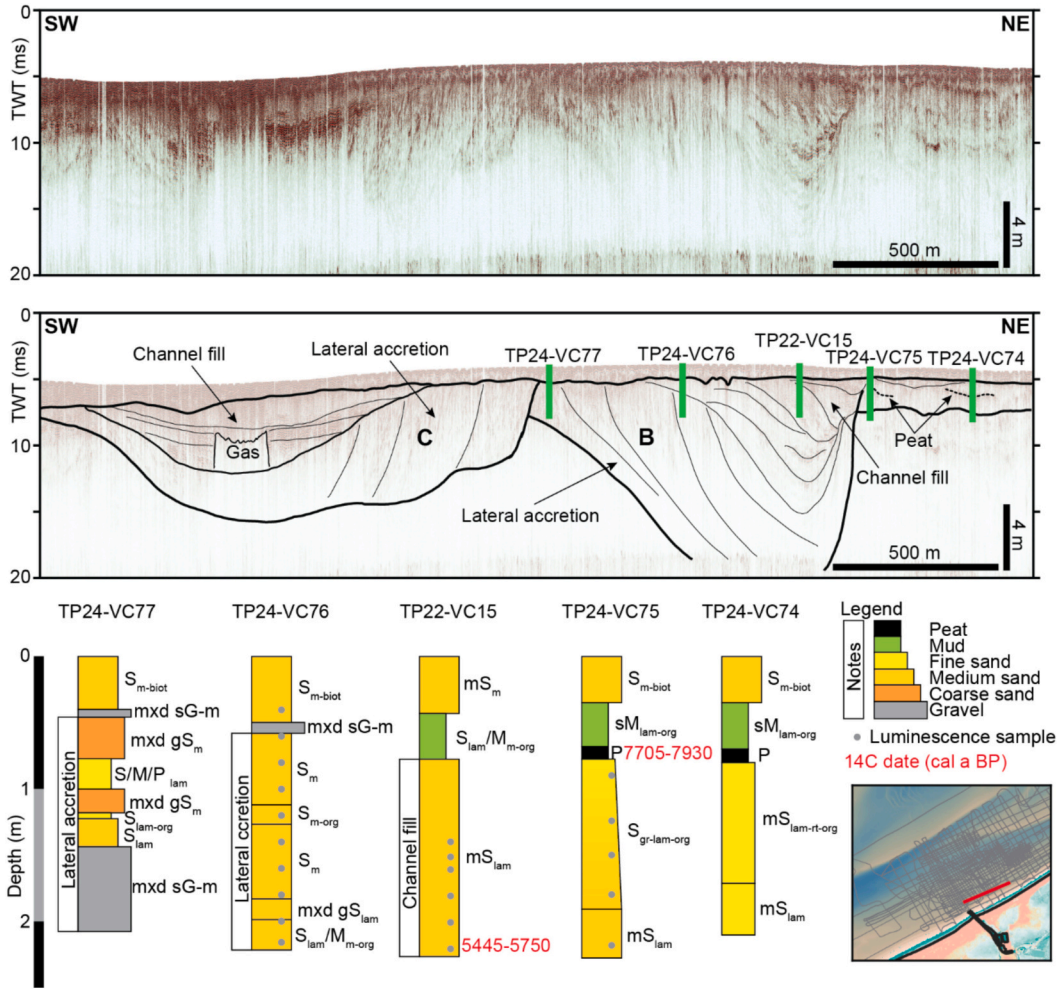

Fig. 6. High-resolution acoustic profile across the study area showing channels B and C, and representative sediment cores. For the codes of the sedimentary facies refer to Supplementary Table S2. Luminescence samples were used for OSL profiling. Pictures of representative cores are included in Supplementary Material (Fig. S3).

(7155–7425 cal a BP) are also considered reworked, because they derive from units directly overlying the disconformity that caps the channels, corresponding to the lowest luminescence values (Fig. 5). In contrast, the only radiocarbon age consistent with the luminescence chronology in this area is that from channel C (core TP22-VC08), yielding an age of 1565–1875 cal a BP (Fig. 7, Table 2).

Taken together, the luminescence profiling, stratigraphic relationships, and selected radiocarbon ages define a clear sequence of tidal inlet activity within the study area. The chronology points to an initial phase centred on channel B (with channel A as a marginal branch), followed by a westward shift to channels E and F, and finally a reoccupation of the eastern sector in channels D and C. The entire system spans several millennia, with ages of the channel fills ranging from 6055 to 6375 cal a BP for channel A to 1565–1875 cal a BP for channel C. The integrated approach not only refines the temporal evolution of the inlet system but also demonstrates the value of luminescence profiling as an efficient screening tool for resolving complex chronologies and detecting potentially reworked radiocarbon ages.

5. Discussion

5.1. Luminescence profiling as a tool to assess complex shallow marine stratigraphy

Reconstructing the chronology of shallow-marine stratigraphies is often hindered by the fragmentary preservation of deposits, the scarcity of datable material, and the frequent reworking of sediments that can compromise radiocarbon and luminescence ages. In such contexts, luminescence profiling provides a valuable complementary approach, offering rapid (measuring one sample in <3 min) and high-resolution stratigraphic information that captures variations across entire sediment cores rather than isolated samples. Gradual trends, abrupt shifts, and inversions in luminescence signals can reflect changes in sedimentation, erosion, and reworking (Munyikwa et al., 2021; Sanderson and Murphy, 2010). While widely applied in terrestrial settings, the use of luminescence profiling in submerged landscapes remains limited (Kinnaird et al., 2022; Munyikwa et al., 2021; Sanderson and Kinnaird, 2019).

In the Belgian nearshore area, luminescence profiling proved particularly powerful for reconstructing the evolution of a submerged relict tidal inlet complex (Fig. 8A). The discontinuous preservation of channel fills and sand body deposits, together with the scarcity of material suitable for radiocarbon dating, would have left large uncertainties if conventional approaches were applied in isolation. By integrating the luminescence profiles with acoustic stratigraphy, we were able to build a three-dimensional relative chronostratigraphic framework that revealed the successive phases of inlet incision, lateral migration, and abandonment (Fig. 8A).

A key advantage of this approach is illustrated by the comparison of channel sequences derived with and without luminescence integration

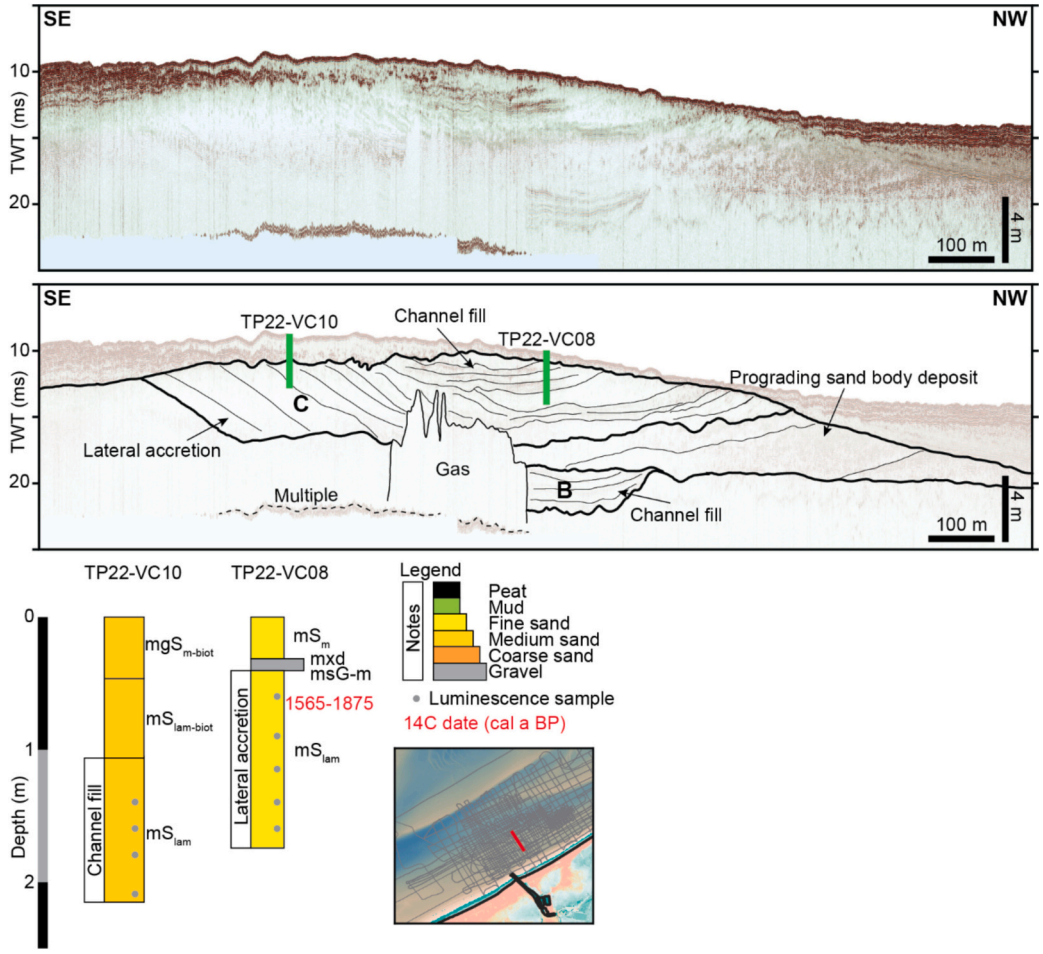

Fig. 7. High-resolution acoustic profile across the study area showing channels B and C, and representative sediment cores. For the codes of the sedimentary facies refer to Supplementary Table S2. Luminescence samples were used for OSL profiling.

Table 1
Morphological characteristics of the channels. Depths are converted to meters (TAW, ~ 2.33 m below present mean sea level) for reference with a mean velocity value of 1600 m/s.

	Depth (ms TWT)		Depth (m TAW)		Longitude (km)	Width (m)		Migration direction
	Max	Mean	Max	Mean		Channel fill	Basal incision	
Channel A	18.6	14.3	−14.9	−11.4	2.8	160–600	300–800	NNW-SSE, N-S
Channel B	27.0	19.1	−21.6	−15.3	4.0	400	1000	SE-NW SSW-NNE
Channel C	18.5	15.0	−14.8	−12.0	2.0	700	1200	NE-SW, SE-NE
Channel D	18.1	13.4	−14.5	−10.7	1.8	250	800	NE-SW
Channel E	16.6	14.3	−13.3	−11.4	3.0	400		N/A
Channel F	19.7	14.2	−15.8	−11.4	2.2	600	2000	NE-SW

(Fig. 9). When relying solely on radiocarbon ages, the inferred evolution of the inlet system appears complex and partly inconsistent, suggesting a sequence of channel activity (B, E, D, B + A, A + F, C, Fig. 9) that conflicts with observed cross-cutting relationships (Fig. 4) and would require multiple channel reactivations and successive west-east shifts in inlet position. In contrast, the integration of luminescence profiles produces a more coherent and stratigraphically consistent sequence (B + A, E, F, D, C, Fig. 9), which better reflects the spatial organisation, evolution and preservation of the system. This discrepancy primarily arises from the reworking of shell material, which can yield anomalously old radiocarbon ages even in the absence of clear macroscopic evidence of reworking. By providing a continuous relative age framework, luminescence profiling enables the identification and exclusion of such outliers, thereby refining the chronological reconstruction. As such, the method not only improves chronological resolution but also acts as a critical quality-control tool in complex shallow-marine settings.

5.2. *Evidence for long-term stability of a Holocene barrier-inlet system*

Tidal inlets, and their associated channels, represent the deepest elements of barrier-inlet systems (FitzGerald et al., 2012; Van Heteren, 2015) and, in case of intense coastal erosion, these systems may represent the only evidence of the former coastline. In present-day analogues, the main ebb channel of tidal inlets is seen to be characterised by a pronounced deepening at the inlet throat, coinciding with the minimum channel width and maximum tidal current velocities (FitzGerald et al., 2012; FitzGerald and Miner, 2013; Hayes and FitzGerald, 2013). The identification of the inlet throat and associated deposits on acoustic data and in the sedimentary archive therefore allows to estimate the position of a former barrier (e.g., Rieu et al., 2005; Ronchi et al., 2019; Storms

Table 2
Radiocarbon ages.

Core	Depth (cm)	Lab code	Material dated	Conventional radiocarbon age	Calibrated age (cal a BP)		Feature dated
					Median	2σ	
TP22-VC08	67.5	Beta-665,312	Marine shell (*Donax* sp.)	2290 ± 30	1726	1565–1875	Channel C
TP22-VC09	73.5	RICH-35146	Marine shell (*Cerastoderma* sp.)	5710 ± 30	5915	5745–6095*	Channel C
TP22-VC11	95	Beta-665,310	Marine shell (*Spisula* sp.)	1100 ± 30	532	420–645	Younger overlying deposits
TP22-VC15	222	Beta-665,309	Marine shell (*Limecola* sp.)	5420 ± 30	5599	5445–5750	Channel B
TP22-VC18	83.5	RICH-35147	Marine shell (*Spisula* sp.)	1270 ± 30	664	540–785	Younger overlying deposits
TP22-VC18	205	RICH-35148	Marine shell (*Cerastoderma* sp.)	6490 ± 30	6760	6600–6935*	Channel D
TP22-VC33	127	RICH-35153	Marine shell (*Cerastoderma* sp.)	4200 ± 30	4095	3915–4275*	Younger overlying deposits
TP22-VC33	166.5	RICH-35154	Marine shell (*Cerastoderma* sp.)	5990 ± 30	6219	6055–6375	Channel A
TP22-VC34_1	130	RICH-35155	Marine shell (*Cerastoderma* sp.)	6980 ± 30	7297	7155–7425*	Younger overlying deposits
TP24-VC75	68.5	RICH-36302	Peat	6984 ± 34	7816	7705–7870 (0.847) 7895–7930 (0.153)	Peat deposits on the side of channel B
TP24-VC81	77	RICH-36303	Marine shell (*Cerastoderma* sp.)	3392 ± 30	3078	2905–3245	Channel F

Samples marked with * are, based on luminescence data, likely reworked.

et al., 2008).

The dimensions of individual channels in our system (Table 1) are similar to those of Holocene inlets identified in other submerged settings (e.g., Hollis et al., 2019; Rieu et al., 2005; Ronchi et al., 2019). What sets the Belgian example apart, however, is the persistence of inlet activity. In contrast to the relatively short-lived inlets described in the Netherlands and the northern Adriatic (Rieu et al., 2005; Ronchi et al., 2018, 2019; Storms et al., 2008), the Belgian coastal plain preserves repeated generations of channel fills and lateral-accretion packages within a confined sector that persisted for at least four millennia. This period corresponds to the approximate time span between the age obtained from the infill of inlets, represented by the oldest channel B, 5445–5750 cal a BP (core TP22-VC15, Fig. 6, Table 2), and the youngest channel C, 1565–1875 cal a BP (core TP22-VC08, Fig. 7, Table 2). However, this could even represent a longer time if the age obtained from channel A, a side branch of channel B situated farther offshore and dated to 6055–6375 cal a BP (TP22-VC33, Fig. 5, Table 2), or the peat deposits cut by channel B, dating to 7705–7930 cal a BP (TP24-VC75, Fig. 6, Table 2), are considered. Nonetheless, this endurance points to the presence of a stable barrier system on both sides of the inlet, constraining its position, and persisting despite rising sea levels and associated erosion.

The entire complex in our study area extends across ~7.5 km of coastline (excluding channel A, interpreted as a marginal feature), a spacing comparable to the distance between barrier islands in the modern Dutch Wadden Sea (ca. 4–9.4 km). This similarity in scale reinforces the interpretation that the Belgian system functioned as a mature and stable barrier–inlet complex which developed during the transgressive and highstand stages of the Holocene. The barrier would be located northeast and southwest of the tidal inlet, while the extensive Belgian coastal plain would correspond to the back-barrier area (Fig. 10). The reconstructed barrier positions, based on inlet throat locations, should be regarded as minimum estimates of the former coastline. Inlet throats are typically located within the central portion of barrier–inlet systems and therefore do not constrain the full seaward extent of the barrier, which may have extended further offshore.

5.3. Regional palaeogeographic implications

The reconstruction of the tidal inlet complex identified offshore of Nieuwpoort provides new insights into the Holocene evolution of the Belgian coastal plain by extending palaeogeographic frameworks into the submerged nearshore. The spatio-temporal patterns of inlet activity reconstructed in this study (Fig. 10) complement previous reconstructions from the emerged coastal plain, which document phases of marine influence alternating with periods of peat accumulation and freshwater marsh expansion (Baeteman, 1999, 2013, 2018; Baeteman et al., 2002; Baeteman and Declercq, 2002; Denys and Baeteman, 1995). Comparable Holocene coastal evolution has been documented in the adjacent French coastal plain, where transgression-driven infilling of incised valleys controlled the development of an extensive tidal basin (Margotta et al., 2016).

The oldest preserved inlet generation, represented by channel B and its marginal branch channel A, records the highest luminescence intensities and the deepest incision. This morphology is consistent with the development of a major ebb channel, capturing tidal flow during an early stage of Holocene transgression. Three zones with deeper incisions along the thalweg likely reflect successive positions of the inlet throat, migrating landwards through time (Figs. 4 and 10), although their absolute chronology remains unconstrained. This phase likely corresponds to the period of rapid enlargement of the back-barrier basin under rising sea levels during the Early and Middle Holocene (Denys and Baeteman, 1995), carving a large inlet to provide sufficient accommodation for sustained tidal exchange. Eventually, channel B was filled with sand, coinciding with a westward relocation of inlet activity towards channels E and F (Figs. 4 and 10). The slight overlap between luminescence values of the upper deposits of channel B and sediments associated with channel E (Fig. 8A) indicates that the shift was progressive as channel B was filling.

Radiocarbon dates from the youngest preserved infill of channel B (core TP22-VC15, Table 2, Fig. 6), indicate that this shift likely happened around 5.5–6 cal ka BP, coinciding with the maximum extent of the back-barrier area as indicated by the extensive marine deposits identified in the IJzer palaeovalley (Fig. 1, Baeteman, 2018; Baeteman and Declercq, 2002). However, the geographical position of the tidal inlets identified offshore does not match the location of former tidal inlet

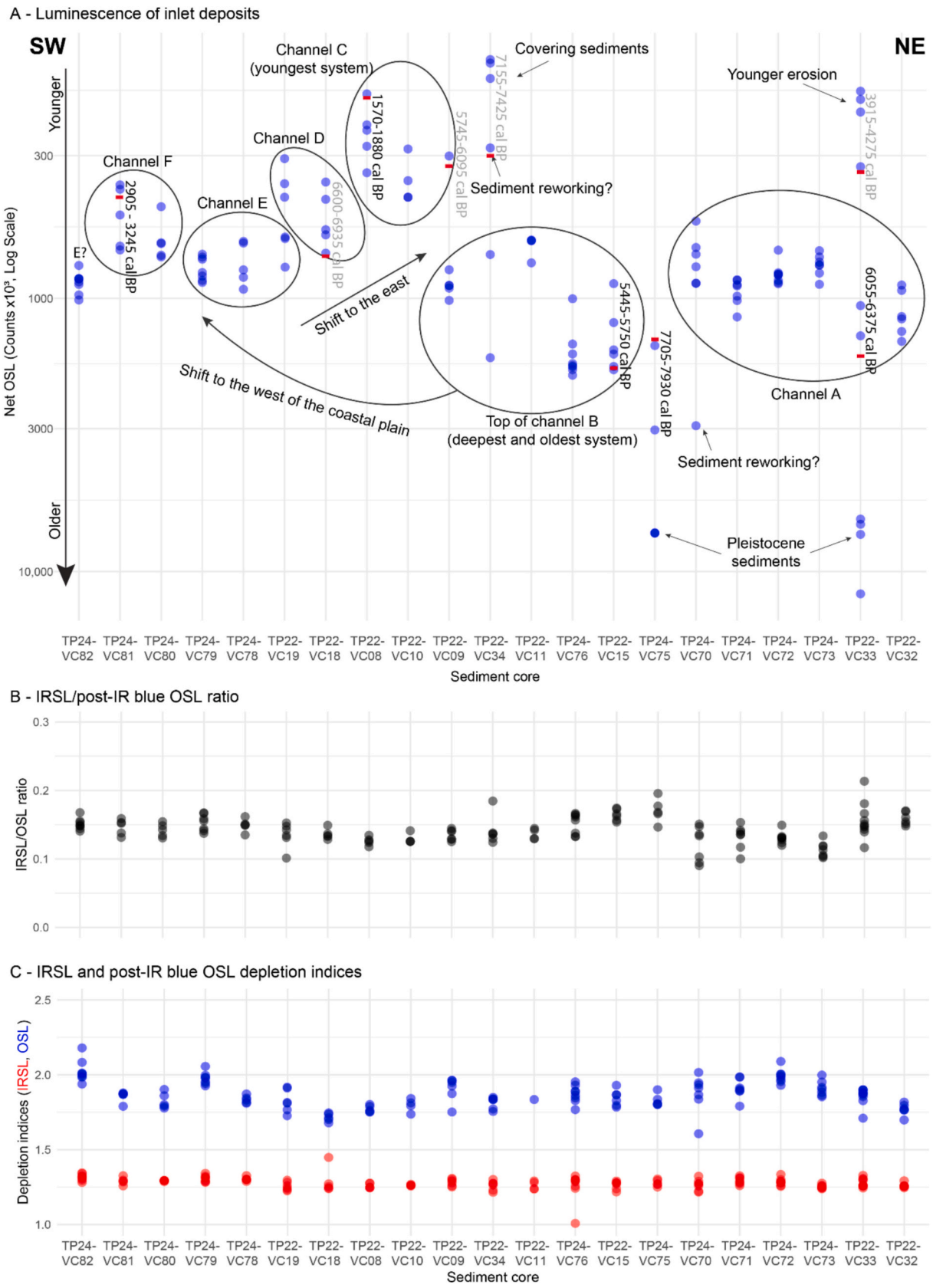

Fig. 8. Luminescence characteristics of bulk sediment samples taken from sand facies of several sediment cores from the tidal inlets. The radiocarbon ages obtained for each deposit are also shown (in black, accepted; in grey, rejected). Sediment cores are shown from west to east along the coast. For detailed location see Fig. 1C. Measurements are included in the Supplementary Table S3. A) Net post-IR blue OSL measurements, in counts. Plotted in reverse scale to display stratigraphic order. In general, the higher the counts the older the deposits. Horizontal red lines indicate the approximate position in the sequence of the radiocarbon ages. B) IRSL/post-IR blue OSL ratio. C) IRSL and post-IR blue OSL depletion indices.

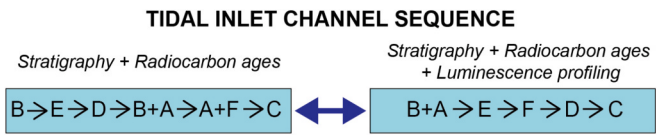

Fig. 9. Tidal inlet channel sequences reconstructed with two different approaches. Using stratigraphy and radiocarbon ages alone (left) produces a more complex and less constrained succession, whereas integrating luminescence profiling (right) refines the temporal ordering of channel fills and improves the internal consistency of the reconstruction.

systems proposed in previous palaeogeographic reconstructions (e.g., Baeteman, 1999, 2013, 2018; Baeteman and Declercq, 2002; Mathys, 2009). In particular, we find no evidence of the seaward continuation of the IJzer palaeovalley (in red on Fig. 1), which near the coast has been mapped as a 4 km wide feature cutting down to −18 m TAW (Baeteman and Declercq, 2002). This IJzer palaeovalley has previously been interpreted as a major conduit for marine influence towards the inland and would have turned into an estuary and a large tidal inlet once the coastal plain was flooded (Baeteman and Declercq, 2002). Instead, in our study, we observe that channel B, the largest and deepest feature in this sector, appears to be the main conduit for water exchange between the back-barrier and the North Sea. Given the absence of any alternative offshore expression of the IJzer palaeovalley, we interpret channel B as representing the seaward continuation of the IJzer estuarine system. Through this connection, it would have linked the offshore inlet to the extensive network of tidal channels preserved in the now-emerged coastal plain. Additionally, previous reconstructions of the Belgian coastal plain (e.g. Baeteman and Declercq, 2002; Mathys, 2009) placed the barrier system for this period closer to the present-day coastline. However, these reconstructions are primarily based on onshore data and, as acknowledged in those studies, the position of the barrier and associated inlets in the nearshore zone remains poorly constrained. Our offshore data provide new constraints on the location of the barrier-inlet system, suggesting that it was situated further seaward than previously inferred (Fig. 10).

This reinterpretation has significant implications for the study of human-landscape interactions and the understanding of archaeological and historical evidence, which rely heavily on terrestrial-based palaeogeographic reconstructions (e.g., Baeteman, 2018; Ervynck et al., 1999; Lehouck and Thoen, 2012; Termote, 2008; Tys, 2013; Verhulst, 1995). Our results indicate that the coastline during the Middle and Late Holocene was located at least 2 km further offshore than previously inferred, implying that substantially larger areas of the present-day nearshore were subaerial or part of the barrier system. This has direct consequences for the reconstruction of settlement patterns, resource exploitation, and accessibility, as areas previously interpreted as marine may in fact have been habitable or used for economic activities. In addition, the long-term persistence of inlet activity within a confined coastal sector suggests a relatively stable configuration of tidal exchange zones, which would have influenced navigation routes, connectivity between inland and marine environments, and the location of favourable settlement areas. The mismatch between offshore evidence and published land-based reconstructions highlights the limitations of the latter, as they rely mostly on discontinuous coring records and a relatively low data density in the coastal area (Baeteman and Declercq, 2002). Our results therefore underscore the critical need to integrate investigations across the land-sea boundary and to revisit existing datasets. In particular, a reanalysis of coastal plain cores using new luminescence profiling methods could provide the resolution required to reconcile onshore and offshore records, ultimately yielding more robust palaeogeographic reconstructions of the Holocene coastal evolution in Belgium.

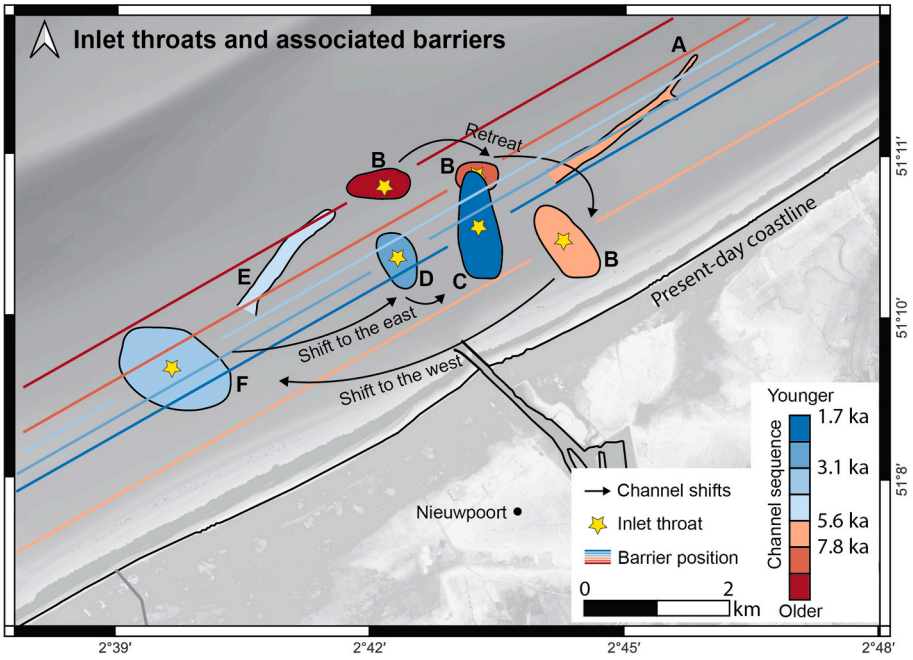

Fig. 10. Reconstruction of the main tidal inlet throats and associated barrier positions in the central Belgian nearshore zone. Coloured polygons represent the interpreted locations of preserved inlet throats (B—F), and solid coloured lines show inferred barrier positions at different stages of coastal evolution. Black arrows indicate the overall eastward and westward shifts in inlet activity. Channel E does not exhibit clear sedimentological or geomorphologic evidence for identifying an inlet throat and is therefore omitted. Barrier orientation cannot be reliably inferred from inlet geometry alone; it is plotted here parallel to the present-day coastline for visual reference. The ages shown in the legend represent approximate central values of the calibrated radiocarbon age ranges for each inlet, used here to provide a relative temporal framework for the inlet–barrier evolution: 7.8 ka corresponds to peat deposits in core TP24-VC75 with an age of 7705–7930 cal a BP, 5.6 ka corresponds to deposits at the top of channel B in core TP22-VC15 with an age of 5445–5750 cal a BP, 3.1 ka corresponds to the deposits at the top of channel F in core TP24-VC81 with an age of 2905–3245 cal a BP, and 1.7 ka was obtained from sediments at the top of channel C in core TP22-VC08 with an age of 1565–1875 cal a BP. Barrier positions derived from inlet throats represent minimum coastline estimates, as the full seaward extent of the barrier cannot be constrained.

The subsequent evolution, from channel B to the younger channels E, F and D, reveals a general trend towards shallower inlet throats with widespread deposits (Table 1), most pronounced for channel F (Fig. 4). A radiocarbon age from the youngest preserved fill in channel F (core TP24-VC81, Table 2, Fig. 3) indicates that this change in the morphology took place before ca. 3.1 cal ka BP. At this time, sedimentary records from the IJzer palaeovalley onshore show a major environmental shift: between 5500 and 4500 and 2250–2000 cal a BP a predominantly tidal environment progressively transformed into a freshwater marsh with widespread peat accumulation (Baeteman, 1999, 2013, 2018). This reflects a reduction in the back-barrier accommodation space as some areas silted up and became supratidal, decreasing the tidal prism (van der Spek, 1995). This evolution agrees with the offshore trend of progressively shallower inlets (Figs. 3 and 6). This period also coincides with a major deceleration in RSL rise, from 2.5 m/kyr to 0.7 m/kyr around 5500–5000 cal a BP (Denys and Baeteman, 1995). Reduced RSL rise favours barrier stability and progradation, promoting inlet migration (FitzGerald et al., 2012; Hayes and FitzGerald, 2013; Van Heteren, 2015). The overlapping luminescence values of channel E, F and D (Fig. 8A) likely record these cyclical phases of abandonment, reactivation, and lateral adjustment within a broad, dynamic inlet complex.

Subsequently, tidal activity shifted eastward and was established at channel C (Fig. 10). Luminescence signals decrease gradually across this sector, suggesting renewed activity in an area previously occupied by channel B. Several radiocarbon ages from this sector are anomalously old and are interpreted as reworked (Table 2). That said, one age of 1570–1880 cal a BP from channel C is consistent with the luminescence chronology (Fig. 8A), placing this reoccupation in the late Holocene. After ca. 2250–2000 cal a BP, onshore sedimentary records show renewed tidal activity and a partial re-expansion of the tidal basin (Baeteman, 1999, 2013, 2018; Baeteman et al., 2002; Vervust et al., 2025). However, this environmental shift is not reflected offshore as significant changes in the morphology of the tidal inlet, with channel C showing similar width and depth as earlier phases (Table 1), suggesting that although the back-barrier system evolved, these changes had limited impact on the tidal prism through the tidal inlet.

The preservation of multiple generations of channel fills within a confined coastal sector provides a rare record of an inlet system that remained as a persistent yet highly dynamic feature in the coastal landscape, shifting position while maintaining continuous tidal exchange (Fig. 10). The extensive prograding sand body deposits associated with these channel phases are interpreted to represent the sedimentary expression of a coupled inlet-delta-barrier system: deposits located seaward of and directly associated with the inlet channels are consistent with remnants of ebb-tidal deltas, likely including swash platforms and bar complexes developed in front of the inlet throat (Fig. 4). In contrast, laterally adjacent sand bodies are interpreted as barrier or spit-related deposits formed through alongshore sediment transport and lateral accretion along the margins of the inlet (Figs. 3 and 4).

Such an interpretation reflects the strong morphodynamic coupling between ebb-tidal deltas and adjacent barrier systems, where sediment is continuously exchanged between the inlet throat, swash platforms, and barrier segments (FitzGerald et al., 2012; Hayes and FitzGerald, 2013). Studies of the present-day Ameland ebb-tidal delta in the Netherlands have shown that such platforms (like the Bornrif Shoal) are relatively stable in the long term (Pearson et al., 2022) and therefore have a high preservation potential. The internal structures of prograding sand bodies observed in our study reveal a dominant migration direction to the east and southeast, indicating sediment bypass across the tidal inlet from the western barrier to the eastern coast. This corresponds to a general alongshore transport pattern similar to that of today and confirms modelling results showing that sediment transport along the Belgian coast has remained broadly consistent since ca. 6 ka (van der Molen and de Swart, 2001a, 2001b). Following the classification of Davis and Hayes (1984), the presence of such large ebb-tidal channels with well-developed ebb-tidal deltas further implies that this relict barrier-inlet complex operated within the mixed energy tide-dominated domain. This interpretation has important implications for reconstructing barrier morphology (Davis and Hayes, 1984; FitzGerald and Miner, 2013; Van Heteren, 2015), particularly for inferring the geometry and extent of barrier elements that have since been removed by later erosion.

When the reconstructed inlet geometries are viewed together with the mapped prograding sand bodies and the general morphodynamics of barrier-inlet systems (FitzGerald et al., 2012; FitzGerald and Miner, 2013; Van Heteren, 2015), the inferred barrier positions (Fig. 10) represent a minimum estimate for the offshore extent of the former coastline. In particular, the Middle and Late Holocene barrier appears to have remained relatively stable at a position at least ca. 2 km seaward of the present-day coast, despite repeated shifts in inlet activity and changes in back-barrier configuration along the coastline. This implies that the Holocene shoreline did not track the inland retreat of the tidal basin but instead persisted offshore as a long-lived barrier complex.

6. Conclusions

This study demonstrates how the integration of high-resolution geophysics, sediment cores, radiocarbon dating and optically stimulated luminescence profiling can resolve the evolution of relict tidal inlets preserved on the continental shelf. The Belgian inlet complex records multiple generations of inlet activity that repeatedly shifted laterally within a confined coastal sector, yet persisted in broadly the same position for at least four millennia. This long-term stability is highly unusual for barrier–inlet systems undergoing Holocene transgression, and it implies that the coastline remained at least 2 km seaward of the present-day shore for most of the Middle and Late Holocene. Luminescence profiling proved essential for establishing a robust chronostratigraphy, enabling the identification of reworked radiocarbon ages and reducing chronological uncertainty in this dynamic shallow-marine environment. By providing the first offshore evidence of processes previously recognised only on land, our results provide a critical counterpart to reconstructions of the Belgian coastal plain and underscore the importance of integrating offshore and onshore records. Together, these findings highlight the exceptional preservation potential of tidal inlets on low-gradient continental shelves and underscore the value of integrated stratigraphic and geochronological approaches for reconstructing coastal evolution.

Acknowledgements

The project: ‘TESTEREP: The evolution of the Flemish seascape (5000 BP-present) – Testerep reconstructed for policymaking and public engagement’ is part of the Strategic Basic Research (SBO) program of the Research Foundation - Flanders (FWO) and ran from 1 October 2021 to September 30, 2025 (Ref. S007522N). The crew of RV *Simon Stevin* and DAB Vloot and the crew of the *Last Freedom* are acknowledged for their support in performing the research at sea. Our special thanks go to Jan Vermaut and Wouter Blomme, whose skilled technical support during the offshore coring operations greatly contributed to the success of this study. S&P Global is acknowledged for granting us an academic license for the use of Kingdom Geoscience.

Appendix A. Supplementary data

Supplementary data to this article can be found online at https://doi.org/10.1016/j.geomorph.2026.110332.

References

Allen, G.P., Posamentier, H.W., 1993. Sequence stratigraphy and facies model of an incised valley fill; the Gironde Estuary, France. J. Sediment. Res. 63, 378–391. https://doi.org/10.1306/D4267B09-2B26-11D7-8648000102C1865D.

Baeteman, C., 1999. The holocene depositional history of the IJzer palaeovalley (Western Belgian coastal plain) with reference to the factors controlling the formation of intercalated peat beds. Geol. Belg. 2, 39–72. https://doi.org/10.20341/gb.2014.010.

Baeteman, C., 2005. How subsoil morphology and erodibility influence the origin and pattern of late Holocene tidal channels: case studies from the Belgian coastal lowlands. Quat. Sci. Rev. 24, 2146–2162. https://doi.org/10.1016/j.quascirev.2004.11.017.

Baeteman, C., 2013. History of research and state of the art of the Holocene depositional history of the Belgian coastal plain. In: Landscapes or Seascapes?, Comparative Rural History of the North Sea Area. Brepols Publishers, pp. 11–29. https://doi.org/10.1484/M.CORN.1.101546.

Baeteman, C., 2018. The coastal plain of Belgium, joint product of natural processes and human activities. In: Demoulin, A. (Ed.), Landscapes and Landforms of Belgium and Luxembourg, World Geomorphological Landscapes. Springer International Publishing, Cham, pp. 313–334. https://doi.org/10.1007/978-3-319-58239-9_19.

Baeteman, C., Declercq, P.-Y., 2002. A synthesis of early and middle holocene coastal changes in the western Belgian lowlands. Belgeo 77–108. https://doi.org/10.4000/belgeo.15994.

Baeteman, C., Scott, D.B., Van Strydonck, M., 2002. Changes in coastal zone processes at a high sea-level stand: a late Holocene example from Belgium. J. Quat. Sci. 17, 547–559. https://doi.org/10.1002/jqs.707.

Belknap, D.F., Kraft, J.C., 1981. Preservation potential of transgressive coastal lithosomes on the U.S. Atlantic shelf. Mar. Geol. 42, 429–442. https://doi.org/10.1016/0025-3227(81)90173-0.

Belknap, D.F., Kraft, J.C., 1985. Influence of antecedent geology on stratigraphic preservation potential and evolution of Delaware's barrier systems. Mar. Geol. 63, 235–262. https://doi.org/10.1016/0025-3227(85)90085-4.

Bienzobas Montávez, N., Thirumalai, K., Marino, G., 2024. Shell reworking impacts on climate variability reconstructions using individual foraminiferal analyses. Paleoceanogr. Paleoclimatology 39, e2023PA004663. https://doi.org/10.1029/2023PA004663.

Bogemans, F., Roe, H.M., Baeteman, C., 2016. Incised Pleistocene valleys in the Western Belgium coastal plain: age, origins and implications for the evolution of the Southern North Sea Basin. Palaeogeogr. Palaeoclimatol. Palaeoecol. 456, 46–59. https://doi.org/10.1016/j.palaeo.2016.04.047.

Cartelle, V., García-Moreiras, I., Martínez-Carreño, N., Muñoz Sobrino, C., García-Gil, S., 2022. The role of antecedent morphology and changing sediment sources in the postglacial palaeogeographical evolution of an incised valley: the sedimentary record of the Ría de Arousa (NW Iberia). Glob. Planet. Chang. 208, 103727. https://doi.org/10.1016/j.gloplacha.2021.103727.

Cattaneo, A., Steel, R.J., 2003. Transgressive deposits: a review of their variability. Earth Sci. Rev. 62, 187–228. https://doi.org/10.1016/S0012-8252(02)00134-4.

Davis, R.A., Hayes, M.O., 1984. What is a wave-dominated coast? Mar. Geol. 60, 313–329. https://doi.org/10.1016/0025-3227(84)90155-5.

De Batist, M., 1989. Seismostratigrafie en struktuur van het paleogeen in de Zuidelijke Noordzee. University of Gent.

De Clercq, M., 2018. Drowned Landscapes of the Belgian Continental Shelf: Implications for Northwest European Landscape Evolution and Preservation Potential for Submerged Heritage. Ghent University, Belgium.

De Francesco, C.G., Hassan, G.S., 2008. Dominance of reworked fossil shells in modern estuarine environments: implications for paleoenvironmental reconstructions based on biological remains. PALAIOS 23, 14–23 (doi:20120322134535).

De Haas, T., Pierik, H.J., Van Der Spek, A.J.F., Cohen, K.M., Van Maanen, B., Kleinhans, M.G., 2018. Holocene evolution of tidal systems in the Netherlands: Effects of rivers, coastal boundary conditions, eco-engineering species, inherited relief and human interference. Earth Sci. Rev. 177, 139–163. https://doi.org/10.1016/j.earscirev.2017.10.006.

Demarest, J.M., Kraft, J.C., 1987. Stratigraphic record of quaternary sea levels: implications for more ancient Strata. In: Nummedal, D., Pilkey, O.H., Howard, J.D. (Eds.), Sea-Level Fluctuation and Coastal Evolution, SEPM Society for Sedimentary Geology, pp. 223–239. https://doi.org/10.2110/pec.87.41.0223.

Denys, L., Baeteman, C., 1995. Holocene evolution of relative sea level and local mean high water spring tides in Belgium—a first assessment. Mar. Geol. 124, 1–19. https://doi.org/10.1016/0025-3227(95)00029-X.

Ervynck, A., Baeteman, C., Demiddele, H., Hollevoet, Y., Pieters, M., Schelvis, J., Tys, D., Strydonck, M.V., Verhaeghe, F., 1999. Human occupation because of a regression, or the cause of a transgression? A critical review of the interaction between geological events and human occupation in the Belgian coastal plain during the first millenium AD. In: Probl. Küstenforschung Im Südl. Nord. - Band 26, 26.

Farrell, K.M., Harris, W.B., Mallinson, D.J., Culver, S.J., Riggs, S.R., Pierson, J., Self-Trail, J.M., Lautier, J.C., 2012. Standardizing texture and facies codes for a process-based classification of clastic sediment and rock. J. Sediment. Res. 82, 364–378 (doi:20120626195552).

FitzGerald, D., Buynevich, I., Hein, C., 2012. Morphodynamics and facies architecture of tidal inlets and tidal deltas. In: Davis Jr., R.A., Dalrymple, R.W. (Eds.), Principles of Tidal Sedimentology. Springer, Netherlands, Dordrecht, pp. 301–333. https://doi.org/10.1007/978-94-007-0123-6_12.

FitzGerald, D.M., Miner, M.D., 2013. 8.11 - tidal inlets and lagoons along siliciclastic barrier coasts. In: Shroder, J. (Jack) F. (Ed.), Treatise on Geomorphology, Second edition. Academic Press, Oxford, pp. 270–288. https://doi.org/10.1016/B978-0-12-818234-5.00079-1.

Hayes, M.O., FitzGerald, D.M., 2013. Origin, evolution, and classification of tidal inlets. J. Coast. Res. 69, 14–33. https://doi.org/10.2112/SI_69_3.

Heaton, T.J., Köhler, P., Butzin, M., Bard, E., Reimer, R.W., Austin, W.E.N., Bronk Ramsey, C., Grootes, P.M., Hughen, K.A., Kromer, B., Reimer, P.J., Adkins, J., Burke, A., Cook, M.S., Olsen, J., Skinner, L.C., 2020. Marine20 - the marine radiocarbon age calibration curve (0-55,000 cal BP). Radiocarbon 62, 779–820. https://doi.org/10.1017/RDC.2020.68.

Hein, C.J., FitzGerald, D.M., Carruthers, E.A., Stone, B.D., Barnhardt, W.A., Gontz, A.M., 2012. Refining the model of barrier island formation along a paraglacial coast in the Gulf of Maine. Mar. Geol. 307–310, 40–57. https://doi.org/10.1016/j.margeo.2012.03.001.

Henriet, J.P., De Moor, G., 1989. The Quaternary and Tertiary Geology of the Southern Bight, North Sea.

Hollis, R.J., Wallace, D.J., Miner, M.D., Gal, N.S., Dike, C., Flocks, J.G., 2019. Late Quaternary evolution and stratigraphic framework influence on coastal systems along the north-central Gulf of Mexico, USA. Quat. Sci. Rev. 223, 105910. https://doi.org/10.1016/j.quascirev.2019.105910.

Kinnaird, T., Bates, M., Bateman, R., Srivastava, A., 2022. Constructing sediment chronologies for Doggerland. In: Gaffney, V., Fitch, S. (Eds.), Europe's Lost Frontiers: Volume 1. Context and Methodology, Europe's Lost Frontiers. Archaeopress, Oxford, pp. 165–180. https://doi.org/10.32028/9781803272689.

Le Bot, S., Van Lancker, V., Deleu, S., De Batist, M., Henriet, J., 2003. Tertiary and quaternary geology of the Belgian continental shelf (No. SPSD II). In: Scientific Support Plan for a Sustainable Development Policy.

Lehouck, A., Thoen, H., 2012. De oude bewoning op de duinen: onderzoek naar landschap en bewoning in de Westhoekduinen van ijzertijd tot middeleeuwen. In: Berquin, H. (Ed.), In het zand geschreven. De duinen van de Westhoek : een geschiedenis. Hans Berquin, pp. 131–191.

Margotta, J., Trentesaux, A., Tribovillard, N., 2016. Tidally-modulated infilling of a large coastal plain during the Holocene; the case of the French Flemish Coastal plain. In: Tessier, B., Reynaud, J. (Eds.), Contributions to Modern and Ancient Tidal Sedimentology. Wiley, pp. 243–260. https://doi.org/10.1002/9781119218395.ch14.

Mathys, M., 2009. The Quaternary Geological Evolution of the Belgian continental shelf, southern North Sea. Ghent University, Belgium.

Mitchum Jr., R.M., 1977. Seismic stratigraphy and global changes of sea level, part 11: glossary of terms used in seismic stratigraphy. In: Payton, C.E. (Ed.), Seismic Stratigraphy – Applications to Hydrocarbon Exploration, 26. American Association of Petroleum Geologists Memoir, pp. 135–144. https://doi.org/10.1306/M26490C13.

Mitchum Jr., R.M., Vail, P.R., 1977. Seismic stratigraphy and global changes of sea level, part 7: Seismic stratigraphic interpretation procedure. In: Payton, C.E. (Ed.), Seismic Stratigraphy – Applications to Hydrocarbon Exploration, 26. American Association of Petroleum Geologists Memoir, pp. 135–144.

Mitchum Jr., R.M., Vail, P.R., Samgree, J.B., 1977. Seismic stratigraphy and global changes of sea level, part 6: stratigraphic interpretation of seismic reflections patterns in depositional sequences. In: Payton, C.E. (Ed.), Seismic Stratigraphy – Applications to Hydrocarbon Exploration, 26. American Association of Petroleum Geologists Memoir, pp. 117–133.

van der Molen, J., de Swart, H.E., 2001a. Holocene tidal conditions and tide-induced sand transport in the southern North Sea. J. Geophys. Res. Oceans 106, 9339–9362. https://doi.org/10.1029/2000JC000488.

van der Molen, J., de Swart, H.E., 2001b. Holocene wave conditions and wave-induced sand transport in the southern North Sea. Cont. Shelf Res. 21, 1723–1749. https://doi.org/10.1016/S0278-4343(01)00018-8.

Muñoz Sobrino, C., Castro-Parada, A., Cartelle, V., Martínez-Carreño, N., Delgado, C., Cazás, N., Lázaro, I., García-Gil, S., 2024. Sediment recycling during the Holocene marine transgression in Ría de Vigo (NW Iberia): multiproxy evidence and environmental implications. Quat. Sci. Rev. 344, 109006. https://doi.org/10.1016/j.quascirev.2024.109006.

Munyikwa, K., Kinnaird, T.C., Sanderson, D.C.W., 2021. The potential of portable luminescence readers in geomorphological investigations: a review. Earth Surf. Process. Landf. 46, 131–150. https://doi.org/10.1002/esp.4975.

Nummedal, D., Swift, D.J.P., 1987. Transgressive stratigraphy at sequence-bounding unconformities: some principles derived from holocene and cretaceous examples. In: Nummedal, D., Pilkey, O.H., Howard, J.D. (Eds.), Sea-Level Fluctuation and Coastal Evolution. SEPM Society for Sedimentary Geology, pp. 223–240.

Paquet, F., Thinon, I., Dugué, O., Tessier, B., Benabdellouahed, M., Lasseur, E., Briais, J., Couëffé, R., Guennoc, P., Gaullier, V., 2023. The Central English Channel troughs: major source-to-sink remnants or giant tidal scours? Mar. Pet. Geol. 153, 106303. https://doi.org/10.1016/j.marpetgeo.2023.106303.

Pearson, S.G., Elias, E.P.L., van Prooijen, B.C., van der Vegt, H., van der Spek, A.J.F., Wang, Z.B., 2022. A novel approach to mapping ebb-tidal delta morphodynamics and stratigraphy. Geomorphology 405, 108185. https://doi.org/10.1016/j.geomorph.2022.108185.

Reimer, P.J., Austin, W.E.N., Bard, E., Bayliss, A., Blackwell, P.G., Ramsey, C.B., Butzin, M., Cheng, H., Edwards, R.L., Friedrich, M., Grootes, P.M., Guilderson, T.P., Hajdas, I., Heaton, T.J., Hogg, A.G., Hughen, K.A., Kromer, B., Manning, S.W., Muscheler, R., Palmer, J.G., Pearson, C., Plicht, J. van der, Reimer, R.W., Richards, D.A., Scott, E.M., Southon, J.R., Turney, C.S.M., Wacker, L., Adolphi, F., Büntgen, U., Capano, M., Fahrni, S.M., Fogtmann-Schulz, A., Friedrich, R., Köhler, P., Kudsk, S., Miyake, F., Olsen, J., Reinig, F., Sakamoto, M., Sookdeo, A., Talamo, S., 2020. The IntCal20 northern hemisphere radiocarbon age calibration curve (0–55 cal kBP). Radiocarbon 62, 725–757. https://doi.org/10.1017/RDC.2020.41.

Rieu, R., van Heteren, S., van der Spek, A.J.F., De Boer, P.L., 2005. Development and preservation of a mid-Holocene tidal-channel network offshore the Western Netherlands. J. Sediment. Res. 75, 409–419 (doi:20121219164506).

Romans, B.W., Castelltort, S., Covault, J.A., Fildani, A., Walsh, J.P., 2016. Environmental signal propagation in sedimentary systems across timescales. Earth Sci. Rev. 153, 7–29. https://doi.org/10.1016/j.earscirev.2015.07.012.

Ronchi, L., Fontana, A., Correggiari, A., Asioli, A., 2018. Late Quaternary incised and infilled landforms in the shelf of the northern Adriatic Sea (Italy). Mar. Geol. 405, 47–67. https://doi.org/10.1016/j.margeo.2018.08.004.

Ronchi, L., Fontana, A., Correggiari, A., Remia, A., 2019. Anatomy of a transgressive tidal inlet reconstructed through high-resolution seismic profiling. Geomorphology 343, 65–80. https://doi.org/10.1016/j.geomorph.2019.06.026.

Sanderson, D.C.W., Kinnaird, T.C., 2019. Optically stimulated luminescence dating as a geochronological tool for Late Quaternary sediments in the Red Sea region. In: Rasul, N.M.A., Stewart, I.C.F. (Eds.), Geological Setting, Palaeoenvironment and Archaeology of the Red Sea. Springer International Publishing, Cham, pp. 685–707. https://doi.org/10.1007/978-3-319-99408-6_31.

Sanderson, D.C.W., Murphy, S., 2010. Using simple portable OSL measurements and laboratory characterisation to help understand complex and heterogeneous sediment sequences for luminescence dating. Quat. Geochronol. 5, 299–305. https://doi.org/10.1016/j.quageo.2009.02.001.

van der Spek, A.J.F., 1995. Reconstruction of Tidal Inlet and Channel Dimensions in the Frisian Middelzee, a Former Tidal Basin in the Dutch Wadden Sea. In: Tidal Signatures in Modern and Ancient Sediments. John Wiley & Sons, Ltd, pp. 237–258. https://doi.org/10.1002/9781444304138.ch16.

Storms, J.E.A., Weltje, G.J., Terra, G.J., Cattaneo, A., Trincardi, F., 2008. Coastal dynamics under conditions of rapid sea-level rise: 8 Holocene evolution of barrier–lagoon systems on the northern Adriatic shelf (Italy). Quat. Sci. Rev. 27, 1107–1123. https://doi.org/10.1016/j.quascirev.2008.02.009.

Stuiver, M., Reimer, P.J., 1993. Extended 14C data base and revised CALIB 3.0 14C age calibration program. Radiocarbon 35, 215–230. https://doi.org/10.1017/S0033822200013904.

Swift, D.J.P., 1968. Coastal Erosion and Transgressive Stratigraphy. J. Geol. 76, 444–456. https://doi.org/10.1086/627342.

Termote, J., 2008. Dankzij de dijken. De bedijkinggeschiedenis en de inname van de Westelijke Kustvlakte van Vlaanderen. Archikrant 18, 71–98.

Toby, S.C., Duller, R.A., De Angelis, S., Straub, K.M., 2022. Morphodynamic limits to environmental signal propagation across landscapes and into strata. Nat. Commun. 13, 292. https://doi.org/10.1038/s41467-021-27776-6.

Tys, Dries, 2013. The medieval embankment of coastal flanders in context. In: Thoen, E., Borger, G.J., Soens, T., de Kraker, A.M.J., Tys, D., Vervaet, L., Weerts, J.K.T. (Eds.), Landscapes or Seascapes? The History of Coastal Environment in the North Sea Area Reconsidered. Brepols Publishers, Turnhout, pp. 199–239.

Van Heteren, S., 2015. Barrier systems. In: Masselink, G., Gehrels, R. (Eds.), Coastal Environments and Global Change. Wiley, pp. 194–226. https://doi.org/10.1002/9781119117261.ch9.

Verhulst, A., 1995. Landschap en landbouw in middeleeuws Vlaanderen. Gemeentekrediet, Brussel.

Vervust, S., Cartelle, V., Plets, R., Vanbiervliet, Z., 2025. Applying OSL profiling and dating on sediment cores to reconstruct landscape changes: pitfalls and strengths. ArchéoSciences 347–350. https://doi.org/10.4000/14nsu.

Verwaest, T., Dujardin, A., Montreuil, A.-L., Trouw, K., 2022. Understanding coastal resilience of the belgian west coast. Water 14, 2104. https://doi.org/10.3390/w14132104.

Wentworth, C.K., 1922. A scale of grade and class terms for clastic sediments. J. Geol. 30, 377–392. https://doi.org/10.1086/622910.

Zecchin, M., Catuneanu, O., 2013. High-resolution sequence stratigraphy of clastic shelves I: units and bounding surfaces. Mar. Pet. Geol. 39, 1–25. https://doi.org/10.1016/j.marpetgeo.2012.08.015.

Zecchin, M., Catuneanu, O., Caffau, M., 2019. Wave-ravinement surfaces: Classification and key characteristics. Earth Sci. Rev. 188, 210–239. https://doi.org/10.1016/j.earscirev.2018.11.011.